2005 American Control Conference
June 8-10, 2005. Portland, OR, USA

Spacecraft Formation Flying near Sun-Earth L_2 Lagrange Point: Trajectory Generation and Adaptive Output Feedback Control

Hong Wong and Vikram Kapila
Mechanical, Aerospace, and Manufacturing Engineering, Polytechnic University, Brooklyn, NY 11201

Abstract— In this paper, we present a trajectory generation and an adaptive, output feedback control design methodology to facilitate spacecraft formation flying near the Sun-Earth L_2 Lagrange point. Specifically, we create a spacecraft formation by placing a leader spacecraft on a desired Halo orbit and a follower spacecraft on a desired quasi-periodic orbit surrounding the Halo orbit. We develop the nonlinear dynamics of the follower spacecraft relative to the leader spacecraft, wherein the leader spacecraft is assumed to be on a desired Halo orbit trajectory. In addition, we design a formation maintenance controller such that the follower spacecraft tracks a desired trajectory. Specifically, we design an adaptive, output feedback position tracking controller, which provides a filtered velocity measurement and an adaptive compensation for the unknown mass of the follower spacecraft. The proposed control law is simulated for the case of the leader and follower spacecraft pair and is shown to yield semi-global, asymptotic convergence of the relative position tracking errors.

I. Introduction

Equilibrium positions in the restricted three body problem (RTBP) of the Sun-Earth system, known as the Lagrange points, have been exploited as key locations for space-based astronomical observation stations [1], [10]. As seen in Figure 1(a), Lagrange points L_1, L_2, and L_3 are collinear with the Sun and Earth while L_4 and L_5 each combined with the Sun and Earth yields an equilateral triangle. A primary benefit of operating observation stations in the vicinity of the Lagrange points is that spacecraft near these points obtain nearly an unobstructed view of the galaxy, unhindered by the atmospheric and geomagnetic forces.

Spacecraft formation flying (SFF) has the potential to enhance space-based imaging/interferometry missions by distributing mission tasks (usually conducted by a monolithic spacecraft) to many small spacecraft. Incorporating this technology into future space missions near the Sun-Earth Lagrange points can enlarge the sensing aperture and increase versatility of future observation platforms. However, effective utilization of this new technology requires proper design of spacecraft formations and for each spacecraft in the formation to be precisely controlled to maintain a meaningful baseline.

Research supported in part by the National Aeronautics and Space Administration–Goddard Space Flight Center under Grant NGT5-151 and the NASA/New York Space Grant Consortium under Grant 39555-6519.

Spacecraft trajectory designs for single spacecraft missions near the Sun-Earth Lagrange points include Lyapunov and Halo orbits [16], [18], [19]. These periodic trajectories have the characteristic that spacecraft do not require fuel to stay on these orbits. Thus, these periodic trajectories are well suited as locations for a leader spacecraft and a formation of follower spacecraft can be placed in the vicinity of these trajectories. Current literature for formation design near the Sun-Earth L_2 Lagrange point is scarce, with the exception of [9], [13], [17]. In [13], reference trajectories for follower spacecraft are computed using classical orbital elements, resulting in bounded orbits around the leader spacecraft on a periodic orbit. In [17], feedback control is utilized to produce reference trajectories for follower spacecraft. In addition, [9] provides a method of generating reference trajectories for follower spacecraft using a numerical method, where the resulting trajectories are quasi-periodic.

Current approaches for spacecraft control near the L_2 Lagrange point require position and velocity sensors for feedback control purposes [7], [8], [11], [12], [14]. However, exploiting the nonlinear, adaptive, output feedback control design methodologies of [3], [6], [15] to control spacecraft near the L_2 Lagrange point eliminates the need for velocity sensors, thus reducing the cost and mass of the spacecraft.

In this paper, we develop a leader-follower spacecraft formation, where the leader spacecraft is on a periodic, Halo orbit around the L_2 Lagrange point in the Sun-Earth system and the follower spacecraft is to track a desired relative trajectory. Specifically, in Section II, we develop the dynamics of the follower spacecraft relative to the leader spacecraft. Next, in Section III, we design a desired quasi-periodic relative trajectory for the follower spacecraft in the spirit of [9]. In contrast to [9], our trajectory design exploits the analytical properties of the quasi-periodic relative trajectories to characterize spacecraft formations using a parameter set. In Section IV, we formulate a trajectory tracking control problem. In Section V, we develop an adaptive, output feedback control algorithm to enable the follower spacecraft to track this desired quasi-periodic relative trajectory. In Section VI, we provide illustrative simulations to demonstrate the efficacy of the proposed trajectory generation and control design schemes. Finally, in Section VII, we give some concluding remarks.

II. System Model

In this section, we develop a nonlinear model characterizing the position dynamics of the follower spacecraft

relative to the leader spacecraft near the L_2 Lagrange point in the Sun-Earth system. Referring to Figure 1, we assume that the Earth and the Sun rotate in a circular orbit around the Sun-Earth system barycenter (center of mass) with a constant angular speed ω. In addition, we attach an inertial coordinate system $\{X, Y, Z\}$ to the Sun-Earth system barycenter and a rotating, right-handed coordinate frame $\{x_{L_2}, y_{L_2}, z_{L_2}\}$ to the L_2 Lagrange point with the x_{L_2}-axis pointing along the direction from the Sun to the Earth, the z_{L_2}-axis pointing along the orbital angular momentum of the Sun-Earth system, and the y_{L_2}-axis being mutually perpendicular to the x_{L_2} and z_{L_2} axes, and pointing in the direction that completes the right-handed coordinate frame.

A. Dynamics of a Spacecraft Relative to the L_2 Lagrange Point

In order to describe the dynamics of a spacecraft formation near the L_2 Lagrange point, we must first describe the dynamics of a spacecraft relative to the L_2 Lagrange point. To do so, let $q(t) \triangleq [x \quad y \quad z]^T \in \mathbb{R}^3$ denote the position vector from the spacecraft to the L_2 Lagrange point, expressed in the $\{x_{L_2}, y_{L_2}, z_{L_2}\}$ coordinate frame. In addition, let $R_{S\to s}(t) \in \mathbb{R}^3$ and $R_{E\to s}(t) \in \mathbb{R}^3$ denote the position vectors from the Sun and Earth, respectively, to the spacecraft. Finally, let R_{L_2}, R_E, and R_S denote the distances between the Sun-Earth system barycenter and the L_2 Lagrange point, the Earth, and the Sun, respectively. Then, the mathematical model describing the position of a spacecraft relative to the L_2 Lagrange point is given by [21]

$$m\ddot{q} + C\dot{q} + N(q, s) = u, \tag{1}$$

where m is the mass of the spacecraft, $C \in \mathbb{R}^{3\times 3}$ is a Coriolis-like matrix defined as $C \triangleq 2m\omega \begin{bmatrix} 0 & -1 & 0 \\ 1 & 0 & 0 \\ 0 & 0 & 0 \end{bmatrix}$, $N \in \mathbb{R}^3$ is a nonlinear term consisting of gravitational effects and inertial forces

$$N \triangleq m \begin{bmatrix} \frac{\mu_S (x+R_{L_2}+R_S)}{\|R_{S\to s}\|^3} + \frac{\mu_E (x+R_{L_2}-R_E)}{\|R_{E\to s}\|^3} - \omega^2 (x + R_{L_2}) \\ \frac{\mu_S\ y}{\|R_{S\to s}\|^3} + \frac{\mu_E\ y}{\|R_{E\to s}\|^3} - \omega^2 y \\ \frac{\mu_S\ z}{\|R_{S\to s}\|^3} + \frac{\mu_E\ z}{\|R_{E\to s}\|^3} \end{bmatrix},$$

and $u(t) \in \mathbb{R}^3$ is the thrust control input to the spacecraft. Furthermore, the constants μ_E and μ_S in the definition of N are defined as $\mu_E \triangleq GM_E$ and $\mu_S \triangleq GM_S$, respectively, where G is the universal gravitational constant, M_E is the mass of the Earth, and M_S is the mass of the Sun.

B. Halo Orbit Trajectory

In this subsection, we describe a method to generate thrust-free, periodic trajectories around the L_2 Lagrange point in the form of Halo orbits. We present a succinct overview of a numerical algorithm to generate these periodic trajectories. Additional details on the generation of these periodic trajectories can be found in [16], [18], [19].

One numerical method [19] of generating thrust-free periodic orbits around the L_2 Lagrange point in the Sun-Earth system involves finding a proper set of position and velocity initial conditions to propagate the spacecraft dynamics of (1), with the control thrust u set to zero. First, the Poincaré-Lindstedt method is used to find a high order analytic approximation to a periodic trajectory in the neighborhood of the L_2 Lagrange point. Next, the initial conditions, based on the Poincaré-Lindstedt method, are used as an initial seed in a numerical algorithm to find a better set of initial conditions leading to a periodic trajectory. This numerical algorithm applies a Taylor series expansion to the spacecraft states with respect to the initial conditions and time and truncates higher order terms, such that for Halo orbits the result is a set of 3 linear equations with 4 unknown variables. Families of orbits can be characterized by fixing one of the unknown variables so that the result gives an equal number of equations to unknowns. Solving the aforementioned linear matrix equation and using the result to update the previous set of initial conditions, we obtain a new initial condition guess.

The spacecraft dynamics are then propagated using the new updated set of initial conditions to verify trajectory periodicity. If the trajectory is sufficiently close to being periodic, then the initial conditions can be used for further simulation, else the above numerical algorithm is used to solve for a new set of initial conditions. Since the collinear Lagrange points are inherently unstable [19], long-term propagation of spacecraft dynamics using the initial conditions obtained in the above manner is futile. However, by exploiting the symmetry property of Halo orbits (see below), we can artificially obtain a periodic orbit by computing trajectory information during half of a period and reusing this trajectory data throughout other simulations.

Halo orbits are classified as periodic trajectories that are symmetric with respect to the $\{x_{L_2}, z_{L_2}\}$ plane (i.e., $y_{L_2} = 0$), and are not confined to be in the orbital plane of the Sun and Earth. Halo orbits have the distinguishing characteristic that their projections on the $\{y_{L_2}, z_{L_2}\}$ plane are curves that resemble a Halo. In this paper, we let $q_H(t) = [x_H \ y_H \ z_H]^T \in \mathbb{R}^3$ denote the position vector from a point on a Halo orbit to the L_2 Lagrange point, expressed in the $\{x_{L_2}, y_{L_2}, z_{L_2}\}$ coordinate frame. An initial seed for the numerical algorithm of [19] consists of a spacecraft starting on the $\{x_{L_2}, z_{L_2}\}$ plane with a nonzero initial y_{L_2} and z_{L_2} velocity (i.e., $q_H(0) = [x_H(0) \quad 0 \quad z_H(0)]^T$ and $\dot{q}_H(0) = [0 \quad \dot{y}_H(0) \quad \dot{z}_d(0)]^T$). Updates to the initial x_{L_2} position and y_{L_2} velocity contribute to finding a closed periodic trajectory. In addition, the initial z_{L_2} position determines the size of the Halo orbit. Figure 1(b) shows a typical Halo orbit trajectory around the L_2 Lagrange point.

In this paper, we use Halo orbits as the reference trajectory for the leader spacecraft. The control design framework of [21] can be employed to ensure that the spacecraft dynamics of (1) tracks a Halo orbit reference trajectory. In a subsequent subsection, we will describe the dynamics of the follower spacecraft relative to the leader spacecraft on the Halo orbit. Finally, we denote $R_{S\to H}(t) \in \mathbb{R}^3$ and $R_{E\to H}(t) \in \mathbb{R}^3$ as the position vectors from the Sun and the Earth, respectively, to the Halo orbit.

Remark 2.1: The Halo orbit trajectory satisfies the spacecraft dynamics of (1) under the condition that the spacecraft control input is zero. Moreover, we express

the leader spacecraft dynamics on the Halo orbit as

$$m\ddot{q}_{\mathrm{H}} + C\dot{q}_{\mathrm{H}} + N(q_{\mathrm{H}}, \mathrm{H}) = 0. \quad (2)$$

We note that the Halo orbit is a periodic trajectory with a frequency denoted as ω_{H}.

C. Follower Spacecraft Dynamics

In this subsection, we describe the dynamics of the follower spacecraft relative to the leader spacecraft tracking a no-thrust, periodic Halo orbit trajectory q_{H} without deviating from this orbit for all time. To describe the dynamics of the follower spacecraft, we express the position vector of the follower spacecraft relative to the L_2 Lagrange point in the coordinate frame $\{x_{\mathrm{L}_2}, y_{\mathrm{L}_2}, z_{\mathrm{L}_2}\}$ as $q_{\mathrm{f}_{\mathrm{L}_2}}(t) = \begin{bmatrix} x_{\mathrm{f}_{\mathrm{L}_2}} & y_{\mathrm{f}_{\mathrm{L}_2}} & z_{\mathrm{f}_{\mathrm{L}_2}} \end{bmatrix}^T \in \mathbb{R}^3$. In addition, we denote $R_{\mathrm{S}\to\mathrm{s_f}}(t) \in \mathbb{R}^3$ and $R_{\mathrm{E}\to\mathrm{s_f}}(t) \in \mathbb{R}^3$ as the position vectors from the Sun and Earth, respectively, to the follower spacecraft. Using (1), the follower spacecraft dynamics relative to the L_2 Lagrange point can be expressed as

$$m_{\mathrm{f}}\ddot{q}_{\mathrm{f}_{\mathrm{L}_2}} + C_{\mathrm{f}}\dot{q}_{\mathrm{f}_{\mathrm{L}_2}} + N_{\mathrm{f}_{\mathrm{L}_2}}(q_{\mathrm{f}_{\mathrm{L}_2}}, \mathrm{s_f}) = u_{\mathrm{f}}, \quad (3)$$

where m_{f} is the mass of the follower spacecraft, $C_{\mathrm{f}} \in \mathbb{R}^{3\times 3}$ is a Coriolis-like matrix defined as $C_{\mathrm{f}} \triangleq 2m_{\mathrm{f}}\omega \cdot \begin{bmatrix} 0 & -1 & 0 \\ 1 & 0 & 0 \\ 0 & 0 & 0 \end{bmatrix}$, $N_{\mathrm{f}_{\mathrm{L}_2}} \in \mathbb{R}^3$ is a nonlinear term consisting of gravitational effects and inertial forces defined as $N_{\mathrm{f}_{\mathrm{L}_2}} \triangleq \frac{m_{\mathrm{f}}}{m} N(q_{\mathrm{f}_{\mathrm{L}_2}}, \mathrm{s_f})$, and $u_{\mathrm{f}}(t) \in \mathbb{R}^3$ is the thrust control input to the follower spacecraft.

Next, we define the relative position between the follower and the leader spacecraft $q_{\mathrm{f}}(t) \in \mathbb{R}^3$ as $q_{\mathrm{f}} \triangleq q_{\mathrm{f}_{\mathrm{L}_2}} - q_{\mathrm{H}}$. To obtain the dynamics of the follower spacecraft relative to the leader spacecraft, we differentiate q_{f} with respect to time twice and multiply both sides of the resulting equation by m_{f} to produce

$$m_{\mathrm{f}}\ddot{q}_{\mathrm{f}} = m_{\mathrm{f}}\ddot{q}_{\mathrm{f}_{\mathrm{L}_2}} - m_{\mathrm{f}}\ddot{q}_{\mathrm{H}}. \quad (4)$$

Next, we solve for $\ddot{q}_{\mathrm{H}}$ in (2), multiply the resulting equation by m_{f}, and substitute the result into (4) to yield

$$m_{\mathrm{f}}\ddot{q}_{\mathrm{f}} + C_{\mathrm{f}}\dot{q}_{\mathrm{f}} + N_{\mathrm{f}}(q_{\mathrm{f}}, \mathrm{s_f}) = u_{\mathrm{f}}, \quad (5)$$

where (3) has been used. Note that $N_{\mathrm{f}} \in \mathbb{R}^3$ is a nonlinear term defined as $N_{\mathrm{f}} \triangleq N_{\mathrm{f}_{\mathrm{L}_2}}(q_{\mathrm{f}_{\mathrm{L}_2}}, \mathrm{s_f}) - N_{\mathrm{H}}(q_{\mathrm{H}}, \mathrm{H})$, where $N_{\mathrm{H}} \in \mathbb{R}^3$ is defined as $N_{\mathrm{H}} \triangleq \frac{m_{\mathrm{f}}}{m} N(q_{\mathrm{H}}, \mathrm{H})$.

Remark 2.2: The Coriolis matrix C_{f} satisfies the skew-symmetric property of $x^T C_{\mathrm{f}} x = 0$, $\forall x \in \mathbb{R}^3$.

Remark 2.3: The left-hand side of (5) produces an affine parameterization $m_{\mathrm{f}}\ddot{q}_{\mathrm{f}} + C_{\mathrm{f}}\dot{q}_{\mathrm{f}} + N_{\mathrm{f}}(q_{\mathrm{f}}, \mathrm{s_f}) = Y(\ddot{q}_{\mathrm{f}}, \dot{q}_{\mathrm{f}}, q_{\mathrm{f}}, \mathrm{s_f})m_{\mathrm{f}}$, where m_{f} is the unknown, constant mass of the follower spacecraft and $Y(\cdot) \in \mathbb{R}^3$ is a regression matrix defined as

$$Y \triangleq [Y_1 \; Y_2 \; Y_3]^T, \quad (6)$$

where $Y_1, Y_2, Y_3 \in \mathbb{R}$ are defined as $Y_1 \triangleq \ddot{x}_{\mathrm{f}} - 2\omega\dot{y}_{\mathrm{f}} - \omega^2 x_{\mathrm{f}} + \frac{\mu_{\mathrm{S}}(x_{\mathrm{f}}+x_{\mathrm{H}}+R_{\mathrm{L}_2}+R_{\mathrm{S}})}{\|R_{\mathrm{S}\to\mathrm{s_f}}\|^3} + \frac{\mu_{\mathrm{E}}(x_{\mathrm{f}}+x_{\mathrm{H}}+R_{\mathrm{L}_2}-R_{\mathrm{E}})}{\|R_{\mathrm{E}\to\mathrm{s_f}}\|^3} - \frac{\mu_{\mathrm{S}}(x_{\mathrm{H}}+R_{\mathrm{L}_2}+R_{\mathrm{S}})}{\|R_{\mathrm{S}\to\mathrm{H}}\|^3} - \frac{\mu_{\mathrm{E}}(x_{\mathrm{H}}+R_{\mathrm{L}_2}-R_{\mathrm{E}})}{\|R_{\mathrm{E}\to\mathrm{H}}\|^3}$, $Y_2 \triangleq \ddot{y}_{\mathrm{f}} + 2\omega\dot{x}_{\mathrm{f}} - \omega^2 y_{\mathrm{f}} + \frac{\mu_{\mathrm{S}}(y_{\mathrm{f}}+y_{\mathrm{H}})}{\|R_{\mathrm{S}\to\mathrm{s_f}}\|^3} + \frac{\mu_{\mathrm{E}}(y_{\mathrm{f}}+y_{\mathrm{H}})}{\|R_{\mathrm{E}\to\mathrm{s_f}}\|^3} - \frac{\mu_{\mathrm{S}}\, y_{\mathrm{H}}}{\|R_{\mathrm{S}\to\mathrm{H}}\|^3} - \frac{\mu_{\mathrm{E}}\, y_{\mathrm{H}}}{\|R_{\mathrm{E}\to\mathrm{H}}\|^3}$, and $Y_3 \triangleq \ddot{z}_{\mathrm{f}} + \frac{\mu_{\mathrm{S}}(z_{\mathrm{f}}+z_{\mathrm{H}})}{\|R_{\mathrm{S}\to\mathrm{s_f}}\|^3} + \frac{\mu_{\mathrm{E}}(z_{\mathrm{f}}+z_{\mathrm{H}})}{\|R_{\mathrm{E}\to\mathrm{s_f}}\|^3} - \frac{\mu_{\mathrm{S}}\, z_{\mathrm{H}}}{\|R_{\mathrm{S}\to\mathrm{H}}\|^3} - \frac{\mu_{\mathrm{E}}\, z_{\mathrm{H}}}{\|R_{\mathrm{E}\to\mathrm{H}}\|^3}$, respectively.

III. Spacecraft Formation Design

In this section, we exploit [9] to develop a method of designing reference trajectories for the follower spacecraft relative to the leader spacecraft on the Halo orbit trajectory. Specifically, we present a method of designing quasi-periodic orbits around a nominal Halo orbit. These quasi-periodic orbits will be used as the desired trajectories for the follower spacecraft. Furthermore, we will exploit special characteristics of these quasi-periodic orbits to parameterize spacecraft formations about the leader spacecraft on the Halo orbit.

We begin by expressing the relative position dynamics of (5) in a state-space form, i.e., let $x_1(t) \in \mathbb{R}^3$ be defined as $x_1 \triangleq q_{\mathrm{f}}$ and $x_2(t) \in \mathbb{R}^3$ be defined as $x_2 \triangleq \dot{q}_{\mathrm{f}}$. Then (5) can be written as

$$\dot{X}_{\mathrm{f}} = \begin{bmatrix} \dot{x}_1 \\ \dot{x}_2 \end{bmatrix} = \begin{bmatrix} x_2 \\ -m_{\mathrm{f}}^{-1}\left(C_{\mathrm{f}}x_2 + N_{\mathrm{f}}(x_1, \mathrm{s_f})\right) \end{bmatrix}, \quad (7)$$

where $X_{\mathrm{f}}(t) \triangleq \begin{bmatrix} x_1^T & x_2^T \end{bmatrix}^T \in \mathbb{R}^6$ and we assume that $u_{\mathrm{f}} = 0$, $\forall t \geq 0$. Next, we linearize the nonlinear terms on the right hand side of (7), in the neighborhood of $X_{\mathrm{f}} = 0$, to obtain

$$\dot{X}_{\mathrm{f}} = AX_{\mathrm{f}}, \quad (8)$$

where $A(t) \in \mathbb{R}^{6\times 6}$, defined as $A \triangleq \begin{bmatrix} 0_3 & \mathrm{I}_3 \\ -m_{\mathrm{f}}^{-1}\frac{dN_{\mathrm{f}}(x_1,\mathrm{s_f})}{dx_1}\Big|_{x_1=0} & -m_{\mathrm{f}}^{-1}C_{\mathrm{f}} \end{bmatrix}$, is a time varying matrix with elements that are periodic with time. Note that 0_3 denotes the 3×3 zero matrix, I_3 denotes the 3×3 identity matrix, and $\frac{dN_{\mathrm{f}}(x_1,\mathrm{s_f})}{dx_1}\Big|_{x_1=0}$ denotes the 3×3 Jacobian matrix of $N_{\mathrm{f}}(x_1, \mathrm{s_f})$ evaluated at $x_1 = 0$. The period of oscillation of A is the same as the period of the nominal Halo orbit, i.e., A is periodic with a frequency ω_{H}. Furthermore, the time dependence of A characterizes the dynamics resulting from the linearization of (7) as a nonautonomous, linear differential equation with a periodic A matrix. Consequently, we employ Floquet theory [4] to transform (8) into an autonomous, linear differential equation so as to facilitate an explicit solution of (8).

We begin by introducing the notion of a fundamental matrix [4] of (8) denoted as $\varphi(t) \in \mathbb{R}^{6\times 6}$. Next, we denote the Halo orbit period as T_{H}. Using Floquet theory, we utilize the transformation

$$X_{\mathrm{f}} = PY_{\mathrm{f}}, \qquad Y_{\mathrm{f}} = P^{-1}X_{\mathrm{f}}, \quad (9)$$

where $Y_{\mathrm{f}}(t) \in \mathbb{R}^6$ is a vector composed of the transformed state X_{f} and $P(t) \in \mathbb{R}^{6\times 6}$ is a matrix with elements that are periodic with time [4], to transform the nonautonomous differential equation of (8) into

$$\dot{Y}_{\mathrm{f}} = BY_{\mathrm{f}}, \quad (10)$$

where $B \in \mathbb{R}^{6\times 6}$ is a constant matrix. Following [4], the B matrix can be computed using φ and T_{H} as follows $B = \frac{1}{T_{\mathrm{H}}}\log\left(\varphi^{-1}(0)\varphi(T_{\mathrm{H}})\right)$, where the log function denotes the logarithm of a matrix. Furthermore, the P matrix can be computed using φ and B as follows $P(t) = \varphi(t)e^{-Bt}$. Note that the P matrix is nonsingular $\forall t \in \mathbb{R}$, such that the transformation of (9) is unique [5].

The autonomous, linear differential equation of (10) is equivalent to (8) in the transformed set of coordinates. Furthermore, the eigenvalues of the B matrix are denoted as the characteristic exponents [5], which describe

the stability characteristics of any trajectory that is sufficiently near the nominal Halo orbit. It is observed in [17] that direct computation of the eigenvalues of B results in a pair of hyperbolic eigenvalues, a pair of zero eigenvalues, and a pair of nonzero, pure, imaginary eigenvalues. We denote the pair of hyperbolic eigenvalues as λ_{h_1} and λ_{h_2} and the frequency corresponding to the nonzero, pure, imaginary eigenvalues as ω_{Q}. Next, we perform a coordinate transformation of the form

$$Y_{\mathrm{f}} = TZ_{\mathrm{f}}, \tag{11}$$

where $Z_{\mathrm{f}}(t) \in \mathbb{R}^6$ is a vector composed of the transformed state Y_{f} and $T \in \mathbb{R}^{6\times 6}$ is a time independent, linear transformation matrix, which transforms the B matrix into a modal matrix form given by $\Omega = \mathrm{diag}\left\{\begin{bmatrix} 0 & 1 \\ 0 & 0 \end{bmatrix}, \begin{bmatrix} 0 & 1 \\ -\lambda_{\mathrm{h}_1}\lambda_{\mathrm{h}_2} & (\lambda_{\mathrm{h}_1}+\lambda_{\mathrm{h}_2}) \end{bmatrix}, \begin{bmatrix} 0 & 1 \\ -\omega_{\mathrm{Q}}^2 & 0 \end{bmatrix}\right\}$. Then, (10) is transformed into $\dot{Z}_{\mathrm{f}} = \Omega Z_{\mathrm{f}}$.

Now it is trivial to obtain the following solution for Z_{f} analytically

$$Z_{\mathrm{f}} = \begin{bmatrix} Z_{\mathrm{f}_1} & Z_{\mathrm{f}_2} & Z_{\mathrm{f}_3} & Z_{\mathrm{f}_4} & Z_{\mathrm{f}_5} & Z_{\mathrm{f}_6} \end{bmatrix}^T,\ Z_{\mathrm{f}_i}(t) \in \mathbb{R},\ i = 1,\ldots,6, \tag{12}$$

where $Z_{\mathrm{f}_1} \triangleq Z_{\mathrm{f}_1}(0) + Z_{\mathrm{f}_2}(0)t$, $Z_{\mathrm{f}_2} \triangleq Z_{\mathrm{f}_2}(0)$, $Z_{\mathrm{f}_3} \triangleq \frac{-\lambda_{\mathrm{h}_2} Z_{\mathrm{f}_3}(0) + Z_{\mathrm{f}_4}(0)}{\lambda_{\mathrm{h}_1}-\lambda_{\mathrm{h}_2}} e^{\lambda_{\mathrm{h}_1} t} + \frac{\lambda_{\mathrm{h}_1} Z_{\mathrm{f}_3}(0) - Z_{\mathrm{f}_4}(0)}{\lambda_{\mathrm{h}_1}-\lambda_{\mathrm{h}_2}} e^{\lambda_{\mathrm{h}_2} t}$, $Z_{\mathrm{f}_4} \triangleq \frac{-\lambda_{\mathrm{h}_2} Z_{\mathrm{f}_3}(0) + Z_{\mathrm{f}_4}(0)}{\lambda_{\mathrm{h}_1}-\lambda_{\mathrm{h}_2}} \lambda_{\mathrm{h}_1} e^{\lambda_{\mathrm{h}_1} t} + \frac{\lambda_{\mathrm{h}_1} Z_{\mathrm{f}_3}(0) - Z_{\mathrm{f}_4}(0)}{\lambda_{\mathrm{h}_1}-\lambda_{\mathrm{h}_2}} \lambda_{\mathrm{h}_2} e^{\lambda_{\mathrm{h}_2} t}$, $Z_{\mathrm{f}_5} \triangleq D\cos(\omega_{\mathrm{Q}} t + \phi)$, and $Z_{\mathrm{f}_6} \triangleq -D\omega_{\mathrm{Q}} \sin(\omega_{\mathrm{Q}} t + \phi)$, $Z_{\mathrm{f}_i}(0)$, $i = 1,\ldots,6$, denotes the i^{th} initial condition of the vector Z_{f}, and $D, \phi \in \mathbb{R}$ are parameters that characterize size, location, and shape of the relative trajectory around the nominal Halo orbit. Eq. (12) reveals that the general solution of Z_{f} may not be periodic for arbitrary initial conditions. However, by properly choosing the initial condition $Z_{\mathrm{f}}(0)$ the terms corresponding to the pair of zero eigenvalues and the hyperbolic eigenvalues that produce unstable and/or asymptotically stable motion can be eliminated, thus resulting in periodic motion for Z_{f}. The remaining periodic terms in (12) allow the trajectory designer freedom to choose the parameters $Z_{\mathrm{f}_1}(0)$, D, and ϕ to satisfy mission specifications.

To compute the follower spacecraft trajectory relative to the nominal Halo orbit requires transformation from $Z_{\mathrm{f}} \longrightarrow X_{\mathrm{f}}$ in the form of

$$X_{\mathrm{f}} = PTZ_{\mathrm{f}}, \tag{13}$$

where (9) and (11) have been used. Note that the P matrix is composed of elements which are periodic with respect to time, with frequency ω_{H}, whereas the solution of Z_{f} is composed of elements which are periodic with respect to time, with frequency ω_{Q}. Consequently, the solution of X_{f} is a trajectory with two frequency components ω_{H} and ω_{Q}. It is observed that the frequencies ω_{Q} and ω_{H} are linearly independent, i.e., the condition $a_1\omega_{\mathrm{Q}} + a_2\omega_{\mathrm{H}} = 0$, $a_i \in \mathbb{Z}$, $i = 1, 2$, where $\mathbb{Z}$ is the set of integers, holds only for $a_i = 0$, $i = 1, 2$ (see [2] for details on linearly independent frequencies). Such a trajectory containing linearly independent frequency components is termed as a quasi-periodic trajectory (see [2] for details on quasi-periodic functions). Thus, the X_{f} trajectory has the characteristic of being quasi-periodic. Finally, we utilize X_{f} as the desired trajectory of the follower spacecraft relative to the Halo orbit $q_{\mathrm{d_f}}(t) \in \mathbb{R}^3$, i.e., $\begin{bmatrix} q_{\mathrm{d_f}}^T & \dot{q}_{\mathrm{d_f}}^T \end{bmatrix}^T = X_{\mathrm{f}}$.

Remark 3.1: To facilitate subsequent illustrative examples, we approximate the Halo orbit and the P matrix using Fourier series approximations. Since both q_{H} and P are periodic with the same period, the resulting Fourier series approximations are convergent to the actual forms of q_{H} and P. To compute the time derivatives of q_{H} and P, we analytically differentiate the Fourier series approximations with respect to time. Thus, it follows that $q_{\mathrm{d_f}}$ and its time derivatives, *viz.*, $\dot{q}_{\mathrm{d_f}}$, $\ddot{q}_{\mathrm{d_f}}$, and $\dddot{q}_{\mathrm{d_f}}$ or equivalently $\dot{X}_{\mathrm{f}}$ and $\ddot{X}_{\mathrm{f}}$, are computed using q_{H}, P, and Z_{f}, and their time derivatives, i.e.,

$$\dot{X}_{\mathrm{f}} = \dot{P}TZ_{\mathrm{f}} + PT\dot{Z}_{\mathrm{f}}, \ddot{X}_{\mathrm{f}} = \ddot{P}TZ_{\mathrm{f}} + 2\dot{P}T\dot{Z}_{\mathrm{f}} + PT\ddot{Z}_{\mathrm{f}}, \tag{14}$$

where (13) has been used.

IV. Trajectory Tracking Problem Formulation

In this section, we formulate a control design problem such that the follower spacecraft relative position q_{f} tracks a desired relative position trajectory $q_{\mathrm{d_f}}$, i.e., $\lim_{t\to\infty} q_{\mathrm{f}}(t) - q_{\mathrm{d_f}}(t) = 0$. The effectiveness of this control objective is quantified through the definition of a position tracking error $e(t) \in \mathbb{R}^3$ as

$$e \triangleq q_{\mathrm{f}} - q_{\mathrm{d_f}}. \tag{15}$$

The goal is to construct a control algorithm that obtains the aforementioned tracking result in the presence of the unknown constant follower spacecraft mass m_{f}. We assume that the velocity measurements of the follower spacecraft relative to the leader spacecraft on a nominal Halo orbit are not available for feedback, i.e., $\dot{q}_{\mathrm{f}}$ is unknown.

To facilitate the control development, we assume that the desired trajectory $q_{\mathrm{d_f}}$ and its first three time derivatives are bounded functions of time. Next, we define the follower spacecraft mass estimation error $\tilde{m}_{\mathrm{f}}(t) \in \mathbb{R}$ as

$$\tilde{m}_{\mathrm{f}} \triangleq \hat{m}_{\mathrm{f}} - m_{\mathrm{f}}, \tag{16}$$

where $\hat{m}_{\mathrm{f}}(t) \in \mathbb{R}$ is the follower spacecraft mass estimate.

V. Adaptive Output Feedback Position Tracking Controller

In this section, we design a desired compensation adaptation control law (DCAL) [3] that asymptotically tracks a pre-specified follower spacecraft relative position trajectory, despite the unknown constant follower spacecraft mass m_{f} and the lack of follower spacecraft relative velocity measurements. In order to state the main result of this section, we define auxiliary error variables $\vartheta(t) \in \mathbb{R}^9$ and $r(t) \in \mathbb{R}^{10}$ as $\vartheta \triangleq \begin{bmatrix} e_f^T & e^T & \eta^T \end{bmatrix}^T$ and $r \triangleq \begin{bmatrix} e_f^T & e^T & \eta^T & \tilde{m}_{\mathrm{f}} \end{bmatrix}^T$, respectively. In addition, we define positive constants λ_1, λ_2, and k_η as $\lambda_1 \triangleq \frac{1}{2}\min\{1, m_{\mathrm{f}}, \Gamma^{-1}\}$, $\lambda_2 \triangleq \frac{1}{2}\max\{1, m_{\mathrm{f}}, \Gamma^{-1}\}$, and $k_\eta \triangleq m_{\mathrm{f}}(k-1) - 1$, respectively. Finally, we define a new regression matrix $Y_{\mathrm{d}}(\cdot) \in \mathbb{R}^3$ as $Y_{\mathrm{d}}(\cdot) \triangleq Y(\ddot{q}_{\mathrm{d_f}}, \dot{q}_{\mathrm{d_f}}, q_{\mathrm{d_f}}, \mathrm{s}_{\mathrm{d_f}})$, where the linear parameterization of Remark 2.3 has been used. Note that in the definition of Y_{d}, $R_{\mathrm{S}\to\mathrm{s_{d_f}}}(t) \in \mathbb{R}^3$ and $R_{\mathrm{E}\to\mathrm{s_{d_f}}}(t) \in \mathbb{R}^3$ are denoted as the position vectors from the Sun and Earth, respectively, to the desired trajectory of the follower spacecraft.

A. Velocity Filter Design

To account for the lack of follower spacecraft relative velocity measurements *viz.*, $\dot{q}_{\rm f}$, a filtered velocity error signal $e_f(t) \in \mathbb{R}^3$ is produced using a filter. The following design is based on the framework of [3]. The filter is constructed using the position tracking error e as an input, as shown below

$$e_f = -ke + p, \tag{17}$$

where $k > 0$ is a positive, constant filter gain, $p(t) \in \mathbb{R}^3$ is a pseudo-velocity tracking error generated using

$$\dot{p} = -(k+1)\,p + (k^2+1)e, \quad p(0) = ke(0). \tag{18}$$

To obtain the closed-loop dynamics of e_f, we take the time derivative of the filtered velocity error signal e_f and replace the dynamics of $\dot{p}(t)$ from (18) to obtain

$$\dot{e}_f = -k\eta - e_f + e, \tag{19}$$

where $\eta(t) \in \mathbb{R}^3$ is an auxiliary tracking error variable defined as

$$\eta \triangleq e + \dot{e} + e_f. \tag{20}$$

In addition, rearranging the definition of η gives the closed-loop error dynamics for $\dot{e}(t)$

$$\dot{e} = \eta - e - e_f. \tag{21}$$

B. Open-Loop Auxiliary Tracking Error Dynamics

In this subsection, we develop the open-loop dynamics of the auxiliary tracking error variable η. We begin by differentiating η of (20) with respect to time, multiplying both sides of the resulting equation by $m_{\rm f}$, substituting for $\dot{e}_f$ from (19) and $\dot{e}$ from (21), and rearranging terms to yield

$$m_{\rm f}\dot{\eta} = m_{\rm f}\ddot{q}_{\rm f} - m_{\rm f}\ddot{q}_{\rm d_f} - m_{\rm f}(k-1)\eta - 2m_{\rm f}e_f, \tag{22}$$

where the definition of (15) has been used. Next, we substitute $m_{\rm f}\ddot{q}_{\rm f}$ from (5) into (22) and rearrange terms to obtain

$$\begin{aligned} m_{\rm f}\dot{\eta} &= -m_{\rm f}\ddot{q}_{\rm d_f} - C_{\rm f}\dot{q}_{\rm d_f} + u_{\rm f} - C_{\rm f}\dot{e} - N_{\rm f}(q_{\rm f}, {\rm s_f}) \\ &\quad -m_{\rm f}(k-1)\eta - 2m_{\rm f}e_f, \end{aligned} \tag{23}$$

where $\dot{q}_{\rm f}$ has been replaced by $\dot{e} + \dot{q}_{\rm d_f}$. We add and subtract $N_{\rm f}(q_{\rm d_f}, {\rm s_{d_f}})$ to and from the right hand side of (23) and substitute $\dot{e}$ from (21) to write the open-loop dynamics of η as follows

$$m_{\rm f}\dot{\eta} = -Y_{\rm d}m_{\rm f} + u_{\rm f} - C_{\rm f}\eta - m_{\rm f}(k-1)\eta + \mathcal{X}, \tag{24}$$

where the definition of the desired regression matrix $Y_{\rm d}$ has been used and $\mathcal{X}(t) \in \mathbb{R}^3$ is defined as

$$\mathcal{X} \triangleq C_{\rm f}(e+e_f) + N_{\rm f}(q_{\rm d_f}, {\rm s_{d_f}}) - N_{\rm f}(q_{\rm f}, {\rm s_f}) - 2m_{\rm f}e_f. \tag{25}$$

Remark 5.1: For $\mathcal{X}$ defined in (25), a boundedness condition is required such that a stability result can be formulated. Using the mean value theorem, as in [15], we can bound $\mathcal{X}$ as follows $\|\mathcal{X}\| \le \rho(\|\vartheta\|)\,\|\vartheta\|$, where $\rho(\cdot)$ is some nondecreasing function.

C. Stability Analysis

In this subsection, we present the main theorem to ensure semi-global, asymptotic stability of the position tracking error.

Theorem 5.1: Let $k \in \mathbb{R}$ be a constant, positive, control gain and $\Gamma \in \mathbb{R}$ be a positive constant. Then, the adaptive, output feedback control law consisting of (17), (18), and

$$u_{\rm f} = Y_{\rm d}\hat{m}_{\rm f} + ke_f - e, \tag{26}$$

$$\begin{aligned} \hat{m}_{\rm f} &= \hat{m}_{\rm f}(0) - \Gamma\int_0^t Y_{\rm d}^T(\sigma)\,(e(\sigma) + e_f(\sigma))\,d\sigma - \Gamma Y_{\rm d}^T e \\ &\quad + \Gamma Y_{\rm d}^T(0)e(0) + \Gamma\int_0^t \frac{dY_{\rm d}^T(\sigma)}{d\sigma}e(\sigma)d\sigma, \end{aligned} \tag{27}$$

ensures semi-global asymptotic convergence of the position tracking errors as delineated by $\lim_{t\to\infty} e(t) = 0$, if k is selected such that $k_\eta > \frac{1}{4}\rho^2\left(\sqrt{\frac{\lambda_2}{\lambda_1}}\|r(0)\|\right)$ where $\rho(\cdot)$ is a nondecreasing function.

Proof. We begin by substituting (26) into (24) to obtain the closed-loop dynamics for η

$$m_{\rm f}\dot{\eta} = Y_{\rm d}\tilde{m}_{\rm f} + ke_f - e - C_{\rm f}\eta - m_{\rm f}(k-1)\eta + \mathcal{X}. \tag{28}$$

Next, differentiating (16) with respect to time and using (27) and (20), we obtain the closed-loop dynamics for the spacecraft mass estimation error

$$\dot{\tilde{m}}_{\rm f} = \dot{\hat{m}}_{\rm f} = -\Gamma Y_{\rm d}^T(\sigma)\eta. \tag{29}$$

We define a positive-definite, candidate Lyapunov function as $V \triangleq \frac{1}{2}e_f^Te_f + \frac{1}{2}e^Te + \frac{1}{2}m_{\rm f}\eta^T\eta + \frac{1}{2}\Gamma^{-1}\tilde{m}_{\rm f}^2$. Applying Rayleigh-Ritz's theorem on V results in

$$\lambda_1\|\vartheta\|^2 \le \lambda_1\|r\|^2 \le V \le \lambda_2\|r\|^2. \tag{30}$$

Next, differentiating V with respect to time and substituting the closed-loop dynamics of (19), (21), (28), and (29) into the result, we obtain

$$\dot{V} = -e_f^Te_f - e^Te - m_{\rm f}(k-1)\eta^T\eta + \eta^T\mathcal{X}, \tag{31}$$

where the skew-symmetry property of Remark 2.2 has been used. In addition, utilizing the upper bound on $\mathcal{X}$ to upper bound (31), we get

$$\dot{V} \le -\|\vartheta\|^2 - k_\eta\|\eta\|^2 + \rho(\|\vartheta\|)\,\|\vartheta\|\|\eta\|, \tag{32}$$

where the definition of k_η has been used. Bounding the last two terms on the right hand side of (32) by completing the squares results in

$$\dot{V} \le -\left(1 - \frac{\rho^2(\|\vartheta\|)}{4k_\eta}\right)\|\vartheta\|^2. \tag{33}$$

Note that if k_η is chosen such that $k_\eta > \frac{\rho^2(\|\vartheta\|)}{4}$, then $\dot{V}$ is negative semidefinite, i.e.,

$$\dot{V} \le -\beta\|\vartheta\|^2, \tag{34}$$

where β is some positive constant defined as $\beta \triangleq 1 - \frac{\rho^2(\|\vartheta\|)}{4k_\eta}$. Utilizing (30) yields a sufficient condition for (34) as follows

$$\dot{V} \le -\beta\|\vartheta\|^2, \quad k_\eta > \frac{1}{4}\rho^2\left(\sqrt{\frac{V(t)}{\lambda_1}}\right). \tag{35}$$

Since V is a non-negative function and $\dot{V}$ is a negative semi-definite function, V is a non-increasing function. Thus, $V \in \mathcal{L}_\infty$ as described by $V(r(t)) \leq V(r(0)) < \infty$, $t \geq 0$. Using (30) and $V(r(t)) \leq V(r(0))$, we obtain a sufficient condition for (35)

$$\dot{V} \leq -\beta \|\vartheta\|^2, \quad k_\eta > \frac{1}{4}\rho^2 \left(\sqrt{\frac{\lambda_2}{\lambda_1}} \|r(0)\| \right). \tag{36}$$

From $V \in \mathcal{L}_\infty$, we know that $e_f, e, \eta, \tilde{m}_\mathrm{f} \in \mathcal{L}_\infty$. Since $e, e_f, \eta \in \mathcal{L}_\infty$, it follows from (20) that $\dot{e} \in \mathcal{L}_\infty$; hence, due to the bound of $q_{\mathrm{d_f}}$, $\dot{q}_{\mathrm{d_f}}$, we can use (15), (19), (20), (25), and (28) to conclude that $q_\mathrm{f}, \dot{q}_\mathrm{f}, \dot{e}_f, \dot{\eta} \in \mathcal{L}_\infty$. Similar signal chasing arguments can now be employed to show that all other signals in the closed-loop system remain bounded. Using (34), it can be easily shown that $e, e_f, \eta \in \mathcal{L}_2$. Since $e, e_f, \eta \in \mathcal{L}_\infty$, using Barbalat's Lemma [6], we conclude that $\lim_{t\to\infty} e(t), e_f(t), \eta(t) = 0$. Thus, the result of Theorem 5.1 follows. □

VI. Simulation Results

In this section, we present illustrative examples that incorporate the algorithms presented in Sections III and V. Specifically, we provide details on computing the quasi-periodic trajectories described in Section III. Next, we provide a simulation of the follower spacecraft relative dynamics (5), utilizing the control laws of (17), (18), (26), and (27) so that the follower spacecraft tracks a desired quasi-periodic trajectory relative to a nominal Halo orbit.

In all simulations, we employ the Sun-Earth system circular orbit parameters [19], [20]: $G = 6.671 \times 10^{-11} \frac{\mathrm{m}^3}{\mathrm{kg \cdot s}^2}$, $\omega = 2.73774795629 \times 10^{-3} \frac{\mathrm{rad}}{\mathrm{day}}$, $M_\mathrm{S} = 1.9891 \times 10^{30}\mathrm{kg}$, $M_\mathrm{E} = 5.974 \times 10^{24}\mathrm{kg}$, 1 AU $= 1.496 \times 10^{8}\mathrm{km}$, and $R_{\mathrm{L}_2} = 1.010033599267463$ AU, where 1 AU stands for 1 Astronomical Unit denoting the distance between the Sun and the Earth. Furthermore, we consider that the follower spacecraft has a mass of $m_\mathrm{f} = 1000\mathrm{kg}$. Finally, the distances R_S and R_E can be computed as $R_\mathrm{S} = \frac{M_\mathrm{E}}{M_\mathrm{E}+M_\mathrm{S}} \times 1\mathrm{AU}$ and $R_\mathrm{E} = \frac{M_\mathrm{S}}{M_\mathrm{E}+M_\mathrm{S}} \times 1\mathrm{AU}$, respectively.

A. Quasi-Periodic Trajectory Generation

Applying the numerical algorithm presented in Subsection II-B results in a family of initial conditions for the Halo orbit from which we have selected the following initial condition $q_\mathrm{H}(0) = [-2.61921376240742 \;\; 0 \;\; -0.13648677396294] \times 10^5\mathrm{km}$ and $\dot{q}_\mathrm{H}(0) = [0 \;\; 4.21353617291110 \;\; 0] \times 10^3 \frac{\mathrm{km}}{\mathrm{day}}$. In addition, the Halo orbit period is determined to be $T_\mathrm{H} = 1.135225027876099 \times 10^3\mathrm{day}$. Figure 1(b) shows the Halo orbit relative to the L_2 Lagrange point and its projections onto the $\{x_{\mathrm{L}_2}, y_{\mathrm{L}_2}\}$, $\{x_{\mathrm{L}_2}, z_{\mathrm{L}_2}\}$, and $\{y_{\mathrm{L}_2}, z_{\mathrm{L}_2}\}$ planes. We utilized 25 terms of a Fourier series to approximate the Halo orbit trajectory q_H. The fundamental matrix φ described in Section III is numerically computed using $A(t)$ as follows $\dot{\varphi} = A(t)\varphi$, $\varphi(0) = \mathrm{I}_6$, $\forall t \in [0, T_\mathrm{H}]$. Thus, using $P(t) = \varphi(t)e^{-Bt}$, P is numerically computed $\forall t \in [0, T_\mathrm{H}]$. Next, we compute a Fourier series approximation of P, where we retain 25 terms of the series approximation. This is used with the analytic expression for Z_f to compute $q_{\mathrm{d_f}}$ and its time derivatives analytically from (14).

To show the resulting trajectories of $q_{\mathrm{d_f}}$, given different numerical values for parameters $Z_{\mathrm{f_1}}(0)$, D, and ϕ, we simulated $q_{\mathrm{d_f}}$ using a parameter set: $Z_{\mathrm{f_1}}(0) = 0$, $D = 0.0001$, and $\phi = 0$ rad. By computing the eigenvalues of the B matrix, we determined $\omega_\mathrm{Q} = 6.286301816644046 \times 10^{-5} \frac{1}{\mathrm{day}}$. Figure 2(a) shows the quasi-periodic trajectory relative to the nominal Halo orbit for parameter values of $\phi = 0$, $\phi = \frac{\pi}{4}$, and $\phi = \frac{\pi}{2}$. Figure 2(a) illustrates that changes in ϕ denote changes in the initial position of the spacecraft along a given quasi-periodic trajectory. Next, we simulated $q_{\mathrm{d_f}}$ using a parameter set: $Z_{\mathrm{f_1}}(0) = 0$, $D = 0.0002$, and $\phi = 0$ rad. Figure 2(b) shows the desired quasi-periodic trajectory relative to the nominal Halo orbit. Note that the parameter D determines the size and shape of the desired quasi-periodic trajectory relative to the nominal Halo orbit. We also simulated $q_{\mathrm{d_f}}$ using a parameter set: $Z_{\mathrm{f_1}}(0) = 0.0001$, $D = 0$, and $\phi = 0$ rad. For this parameter set, Figure 3(a) shows a periodic trajectory relative to the nominal Halo orbit with the same period as ω_H. Finally, we simulated $q_{\mathrm{d_f}}$ using a parameter set: $Z_{\mathrm{f_1}}(0) = 0.0001$, $D = 0.0001$, and $\phi = 0$ rad. For this parameter set, Figure 3(b) shows the quasi-periodic trajectory relative to the nominal Halo orbit.

B. Adaptive Output Feedback Control of the Follower Spacecraft

The control law consisting of (17), (18), (26), and (27) was simulated for the follower spacecraft dynamics relative to the leader spacecraft on a nominal Halo orbit (5). When tracking desired quasi-periodic trajectories, we initialized the follower spacecraft with the set of initial conditions given as $q_\mathrm{f}(0) = [-2.61921376240742 \;\; -2.57780484325713 \;\; -0.13648677396294] \times 10^5\mathrm{km}$ and $\dot{q}_\mathrm{f}(0) = [-0.1469110370264 \;\; 42.1353617291110 \;\; -0.1469092330256] \times 10^2 \frac{\mathrm{km}}{\mathrm{day}}$. The control and adaptation gains are obtained through trial and error in order to obtain good performance for the tracking error response. The following resulting gains were used in this simulation $k = 44.97$ and $\Gamma = 9.3 \times 10^5$. In addition, the follower spacecraft mass parameter estimate was initialized to $\hat{m}_\mathrm{f}(0) = 600$ kg. A simulation of the follower spacecraft tracking the desired quasi-periodic trajectory of Figure 2(a) is performed. The trajectory q_f is shown in Figures 4(a) and 4(b). Figure 5 shows the position tracking error e and the pseudo-velocity error e_f. The control input u_f is shown in Figure 6(a). Finally, the follower spacecraft mass estimate $\hat{m}_\mathrm{f}$ is shown in Figure 6(b).

VII. Conclusion

In this paper, we designed desired quasi-periodic trajectories for the follower spacecraft relative to the leader spacecraft on the Halo orbit. The size, location, and shape of these trajectories were characterized by a parameter set. Illustrative simulations were performed to show these parameter characteristics. Next, a Lyapunov design was used to develop an adaptive, output feedback controller, which yielded semi-global, asymptotic convergence of the relative position tracking errors. The control law required only position error measurements while estimating velocity error measurements through a filtering scheme. Simulation results were presented to show good trajectory tracking.

References

[1] http://nssdc.gsfc.nasa.gov/space/isee.html, website of International Sun-Earth Explorers Project Information.

[2] H. Bohr, *Almost Periodic Functions*. Springer, Berlin, 1933.

[3] T. Burg, D. Dawson, J. Hu, and M. de Queiroz, "An Adaptive Partial State Feedback Controller for RLED Robot Manipulators," *IEEE Transaction on Automatic Control*, Vol. 41, No. 7, pp. 1024–1031, 1996.

[4] C. T. Chen, *Linear System Theory and Design*. Oxford University Press, Oxford, NY, 1999.

[5] E. A. Coddington and N. Levinson, *Theory of Ordinary Differential Equations*. McGraw Hill, New York, NY, 1955.

[6] D. M. Dawson, J. Hu, and T. C. Burg, *Nonlinear Control of Electric Machinery*. Marcel Dekker, New York, NY, 1998.

[7] P. Di Giamberardino and S. Monaco, "Nonlinear Regulation in Halo Orbits Control Design," *Proceedings of Conference on Decision and Control,* Tuscan, AZ, pp. 536–541, 1992.

[8] G. Gomez, J. Llibre, R. Martnez, J. Rodrguez-Canabal, and C. Simo, "On the Optimal Station-Keeping Control of Halo Orbits," *Acta Astronautica,* Vol. 15, No. 6, pp. 391–397, 1987.

[9] G. Gomez, J. Masdemont, C. Simo, "Lissajous Orbits around Halo Orbits," *AAS/AIAA Space Flight Mechanics Meeting*, AAS Paper 97-106, 1997.

[10] K. C. Howell, B. T. Barden, R. S. Wilson, and M. W. Lo, "Trajectory Design using a Dynamical Systems approach with Application to Genesis," *Proceedings of the AAS/AIAA Astrodynamics Specialist Conference,* Sun Valley, ID, AAS Paper 97–709, 1997.

[11] K. C. Howell and S. C. Gordon, "Orbit Determination Error Analysis and a Station Keeping Strategy for Sun Earth L_1 Libration Point Orbits," *Journal of Astronautical Sciences,* Vol. 42, pp. 207–228, 1994.

[12] K. C. Howell and H. J. Pernicka, "Station-Keeping Method for Libration Point Trajectories," *Journal of Guidance and Control,* Vol. 16, pp. 151–159, 1993.

[13] F. Y. Hsiao and D. J. Scheeres, "Design of Spacecraft Formation Orbits Relative to a Stabilized Trajectory," *AAS/AIAA Space Flight Mechanics Meeting,* AAS Paper 03-175, 2003.

[14] T. M. Keeter, *Station-Keeping Strategies for Libration Point Orbits: Target Point and Floquet Mode Approaches,* Master's thesis, School of Aeronautics and Astronautics, Purdue University, West Lafayette, IN, 1994.

[15] M. S. de Queiroz, D. Dawson, T. Burg, "Position/Force Control of Robot Manipulators without Velocity/Force Measurements," *International Journal of Robotics and Automation*, Vol. 12, pp. 1–14, 1997.

[16] D. L. Richardson, "Analytic Construction of Periodic Orbits about the Collinear Points," *Celestial Mechanics*, Vol. 22, pp. 241-253, 1980.

[17] D. J. Scheeres, F. Y. Hsiao, and N. X. Vinh, "Stabilizing Motion Relative to an Unstable Orbit: Applications to Spacecraft Formation Flight," *Journal of Guidance, Control, and Dynamics*, Vol. 26, No. 1, pp. 62–73, 2003.

[18] V. Szebehely, *Theory of Orbits*. Academic Press, New York, NY, 1967.

[19] R. Thurman and P. A. Worfolk, *The Geometry of Halo Orbits in the Circular Restricted Three-Body Problem*, Geometry Center Research Report GCG95, University of Minnesota, 1996.

[20] D. A. Vallado, *Fundamentals of Astrodynamics and Applications*. McGraw Hill, New York, NY, 1997.

[21] H. Wong and V. Kapila, "Adaptive Nonlinear Control of Spacecraft Near Sun-Earth L_2 Lagrange Point," *Proceedings of the American Control Conference*, Denver, CO, pp. 1116–1121, 2003.

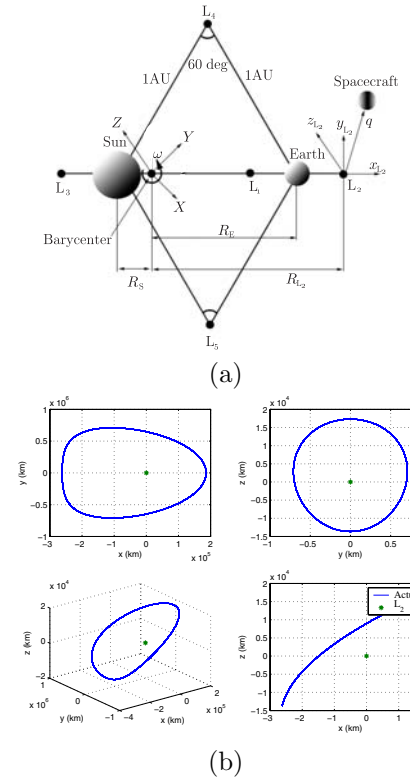

Fig. 1. (a) Sun-Earth system schematic diagram and (b) Halo orbit trajectory of the leader spacecraft relative to the L_2 Lagrange point

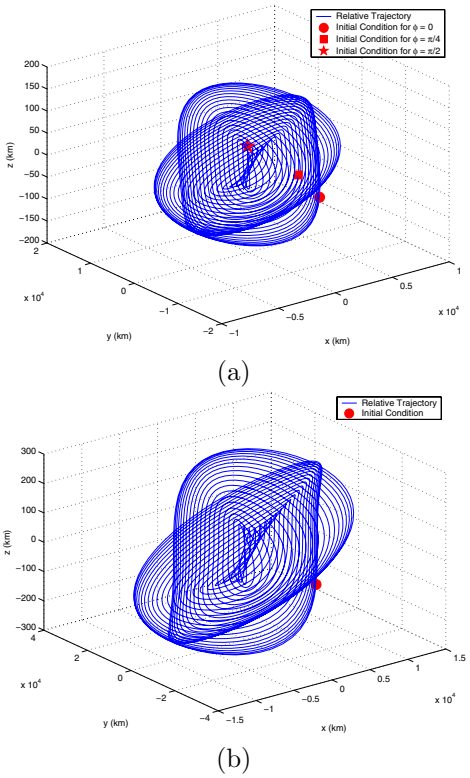

Fig. 2. Trajectory of the follower spacecraft relative to the nominal Halo orbit using: (a) $Z_{f_1}(0) = 0, D = 0.0001, \phi = 0, \phi = \frac{\pi}{4}$, and $\phi = \frac{\pi}{2}$ and (b) $Z_{f_1}(0) = 0, D = 0.0002, \phi = 0$

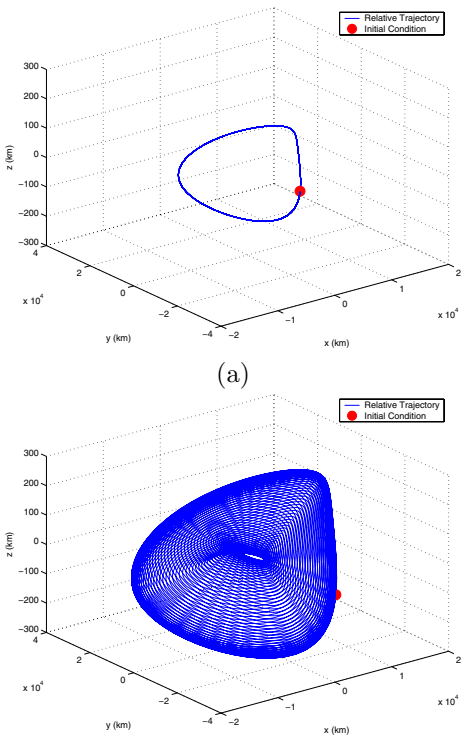

Fig. 3. Trajectory of the follower spacecraft relative to the nominal Halo orbit using: (a) $Z_{f_1}(0) = 0.0001$, $D = 0$, $\phi = 0$ and (b) $Z_{f_1}(0) = 0.0001$, $D = 0.0001$, $\phi = 0$

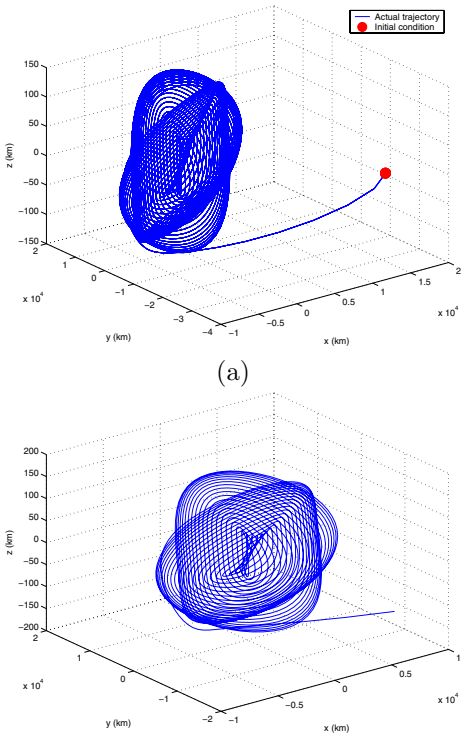

Fig. 4. Trajectory of the follower spacecraft relative to the nominal Halo orbit using: (a) normal view and (b) zoomed in view

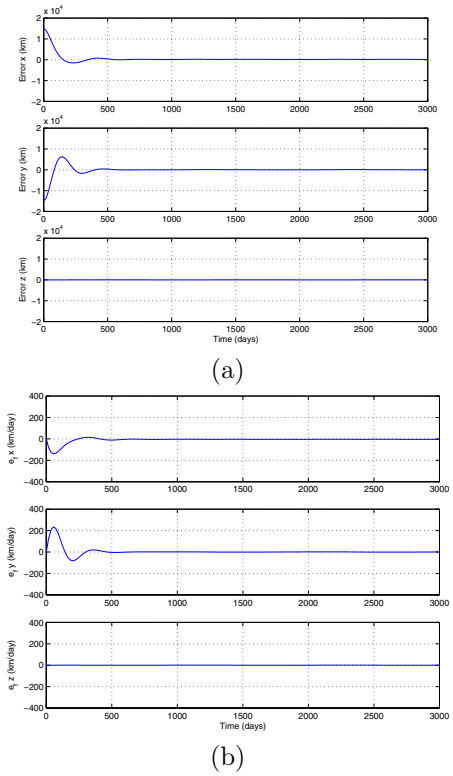

Fig. 5. (a) Position tracking error and (b) filtered velocity error signal

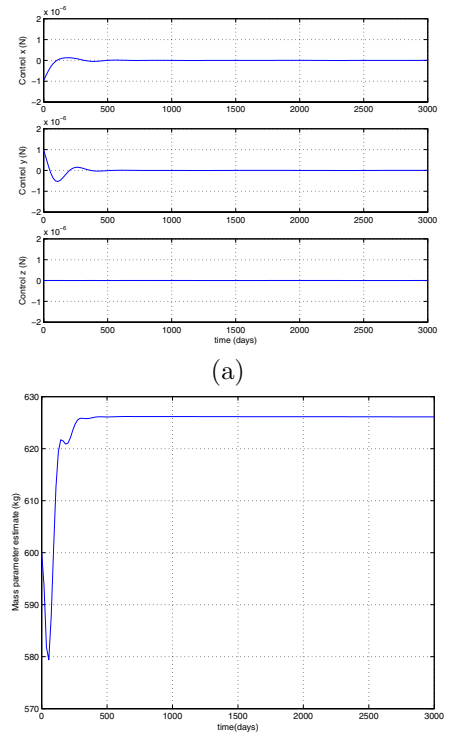

Fig. 6. Follower spacecraft (a) control input and (b) mass parameter estimate